Phys. Med. Biol. **55** (2010) N23–N38 doi:10.1088/0031-9155/55/2/N01

NOTE

The Virtual Family—development of surface-based anatomical models of two adults and two children for dosimetric simulations

Andreas Christ[1], Wolfgang Kainz[2], Eckhart G Hahn[3], Katharina Honegger[1], Marcel Zefferer[1], Esra Neufeld[1,4], Wolfgang Rascher[3], Rolf Janka[3], Werner Bautz[3], Ji Chen[5], Berthold Kiefer[6], Peter Schmitt[6], Hans-Peter Hollenbach[6], Jianxiang Shen[5], Michael Oberle[1], Dominik Szczerba[1], Anthony Kam[7], Joshua W Guag[2] and Niels Kuster[1,4]

[1] Foundation for Research on Information Technologies in Society (IT'IS), Zeughausstr. 43, 8004 Zürich, Switzerland
[2] US Food and Drug Administration (FDA), Center for Devices and Radiological Health (CDRH), Silver Spring, MD 20993, USA
[3] Universitätsklinikum Erlangen, Friedrich-Alexander Universität Erlangen-Nürnberg, 91054 Erlangen, Germany
[4] Swiss Federal Institute of Technology (ETHZ), Rämistr. 101, 8092 Zürich, Switzerland
[5] Department of Electrical and Computer Engineering, The University of Houston, Houston, TX 77204, USA
[6] Siemens Healthcare, MR-Application Development, 91052 Erlangen, Germany
[7] Department of Imaging, Johns Hopkins Bayview Medical Center, Baltimore, MD 21224, USA

E-mail: christ@itis.ethz.ch

Received 13 July 2009, in final form 12 October 2009
Published 17 December 2009
Online at stacks.iop.org/PMB/55/N23

Abstract
The objective of this study was to develop anatomically correct whole body human models of an adult male (34 years old), an adult female (26 years old) and two children (an 11-year-old girl and a six-year-old boy) for the optimized evaluation of electromagnetic exposure. These four models are referred to as the Virtual Family. They are based on high resolution magnetic resonance (MR) images of healthy volunteers. More than 80 different tissue types were distinguished during the segmentation. To improve the accuracy and the effectiveness of the segmentation, a novel semi-automated tool was used to analyze and segment the data. All tissues and organs were reconstructed as three-dimensional (3D) unstructured triangulated surface objects, yielding high precision images of individual features of the body. This greatly enhances the meshing flexibility and the accuracy with respect to thin tissue layers and small organs in comparison with the traditional voxel-based representation of anatomical models. Conformal computational techniques were also applied. The techniques and tools developed in this study can be used to more effectively develop future models and further improve the accuracy of the models for

various applications. For research purposes, the four models are provided for free to the scientific community.

1. Introduction

Anatomical computer models of the human body have been used for more than three decades for dosimetric applications in electromagnetics (EM) (Hand *et al* 2008) and in medical radiation physics (Andreo 1991). Currently, about 20 whole and partial body models of adults and about 14 models of children (from newborn to 14 years of age) are available to the scientific community[8]. Comprehensive overviews can be found in (Caon 2004, Zaidi and Xu 2007, Xu *et al* 2007), and recently, voxel-based models whose dimensions and organ masses correspond to the values defined by the ICRP (2002) were developed (Zankl *et al* 2005). With the exception of a few models, which are based on cryosection images (Ackerman 1998, Kim *et al* 2008), all models were developed from computer tomographic (CT) or magnetic resonance (MR) images of healthy volunteers, patients or cadavers. In comparison with CT imaging, MR tomography yields improved soft-tissue contrast and is therefore preferable for the identification and segmentation of different body tissues and organs. The reliable identification of soft tissues with different dielectric properties is of particular importance in non-ionizing radiation dosimetry, e.g., for the identification of hot spots, which are likely to occur at tissue interfaces with high dielectric contrast (see below).

The image sets of most anatomical body models have been segmented using a fixed spatial resolution (e.g. cubical voxels) over the entire body region, thus limiting anatomical and computational accuracy. Their resolution generally corresponds to the pixel size of the original set of images or to an integer multiple of it. It can range from approximately 0.5 mm $\times$ 0.5 mm $\times$ 1.0 mm for models of newborn children (Nipper *et al* 2002) to more than 5 mm for some adult models. If a coarser resolution is chosen for the segmented model to save computational resources, small anatomical details of the anatomical images are irretrievably lost. Moreover, the thickness of the skin and fat layers, which is an important parameter for the radio frequency (RF) absorption at the surface of the body (Klemm and Troester 2006, Christ *et al* 2006a, 2006b), can only be represented as an integer multiple of the voxel dimensions.

The most prominent numerical methods used in computational dosimetry of electromagnetic fields are based on finite-difference formulations of the underlying differential equations. For the simulation of both RF fields and induced tissue heating, the finite-difference time-domain (FDTD) method in its formulations by Yee (1966) and Patankar (1980) is applied to rectilinear grids to optimally handle large voxel models. However, the use of rectilinear grids imposes restrictions on the geometry in order to reduce the computational uncertainty, e.g., by aligning the conducting structures, such as antennas, with the grid. A typical example is the calculation of the specific absorption rate (SAR) in the head of a cell phone user (Kainz *et al* 2005, Beard *et al* 2006). In order to place the head of an anatomical model next to a cellular phone according to the positions defined in the compliance testing standards (IEEE 2003, IEC 2005), the model must be rotated and resampled according to the computational grid. Resampling of the models is also required if non-uniform meshing is used (Christ *et al* 2002) to save computational expenses. Small anatomical details will usually be lost or thin tissue structures, such as the skin or fat layers, will be corrupted. The representation

[8] The exact number of models is difficult to specify because different models were developed based on the same source data, or partial data sets of different patients or volunteers were combined to develop one complete body model. The stylized models, which consist of generic geometrical shapes and have found their application range in radiation physics, are not considered in this paper.

of the models in the 2.5D 'Compound-Format' (Christ *et al* 2005), which retains the precise outlines of the tissue boundaries of the original slice images in two dimensions, mitigated these problems to a certain extent. It is still, however, not suitable to use novel conformal techniques for EM and thermal FDTD (Benkler *et al* 2008, Neufeld *et al* 2007).

Volumetric or surface description methods, however, provide the basis for the perfect model by converting all tissues to closed three-dimensional (3D) surfaces or boundaries. The surfaces of the tissues can be represented, e.g., as polygonal meshes or by mathematical functions. Non-uniform rational B-splines (NURBS) have been applied to model the human body (Xu *et al* 2000, Xu and Shi 2005) and its dynamics (Segars *et al* 1999, Segars 2001, Segars *et al* 2001). More recently, whole body models of pregnant women (Xu *et al* 2007) and newborn children (Lee *et al* 2007) have been developed based on boundary representation techniques, providing a high level of anatomical details.

2. Objectives

The main parameters for models used in radiation physics are mass and position of the organs as well as their shape and the shape of the body (Zankl *et al* 2002, Staton *et al* 2003). In addition, EM dosimetry requires sound representation of organ interfaces and thin tissue structures. This is particularly important for interfaces with high dielectric contrast, such as skin, fat, bone and muscle tissue (Gabriel *et al* 1996), in order to correctly render reflections, interference effects and hot spots at tissue boundaries with high dielectric contrast, such as skin–fat–muscle interfaces (Schwan and Li 1956, Shapiro *et al* 1968, Kritikos and Schwan 1976, Christ *et al* 2006b). Because of the limited availability of whole body models of children, adult models were often scaled to the anatomical dimensions of children (Gandhi *et al* 1996, Dimbylow 2002). This may introduce uncertainties with respect to the thicknesses of thin tissue layers (skin, skull, subcutaneous adipose tissue, etc) or the proportion and position of body fat. Moreover, scaling can introduce spurious changes in proportions—in particular of the head and the brain—leading to ambiguities in the assessment of the local exposure and has therefore repeatedly been discouraged (Bit-Babik *et al* 2005, Wiart *et al* 2005, 2008).

Hence, the objectives of this study were as follows:

- to develop four novel anatomically correct whole body models of two adults and two children with sizes and body masses close to current worldwide (adults) and German (children) averages[9],
- to preserve the individual anatomical features of the volunteers in order to minimize uncertainties that may arise from scaling or morphing of tissues or organs,
- to represent all tissues and organs as 3D objects consisting of unstructured triangulated surfaces (polygons) in order to overcome the limitations of traditional voxel models with fixed resolution while using a simple and straightforward representation of small anatomical details[10].

In addition to electromagnetics and radiation physics, these models will have a much broader application range in the future, e.g., in virtual patient applications.

[9] Worldwide averages for adults are 1.73 m body height and 77 kg for males and 1.60 m and 67 kg for females (McGee 2005). For girls of eleven years of age and boys of six years of age (section 3.1), German statistics (Kromeyer-Hauschild *et al* 2001) indicate 1.48 m and 37 kg and 1.17 m and 22 kg, respectively. German statistics were chosen for the children because the volunteers for the study were recruited in Germany.

[10] Alternative methods for the numerical representation of organ surfaces, such as NURBS (section 1) allow flexible deformation and scaling of the models. This, however, does not fall into the scope of the present study. An extension for the articulation of the limbs of the models which retains the original masses of the soft tissues is currently under development (Cherubini *et al* 2008).

Table 1. Characteristics of the four anatomical models. The names of the models do not correspond to their real names to protect the identities of the volunteers.

Name[a]	Age (years)	Sex	Height (m)	Mass (kg)	BMI (kg m^{-2})
Duke	34	Male	1.74	70	23.1
Ella	26	Female	1.60	58	22.7
Billie	11	Female	1.46	36	16.7
Thelonious	6	Male	1.17	20	14.2

3. Methods

3.1. MR scans of two adults and two children

3.1.1. Recruitment of the volunteers. To meet the constraints on the models' body masses mentioned in section 2, a retrospective review of existing whole body image sets was conducted, but unsuccessful. Combined partial body image sets could not be used because the models should possess realistic individual features. Consequently, the anatomical models were developed based on image sets of whole body scans of four volunteers (two adults and two children). MR was used instead of CT based on ethical considerations (absence of ionizing radiation) with particular respect to the children and the improved soft tissue contrast of MR, as mentioned above. An ethics committee approved the study protocol, and an appropriate liability insurance was procured. The volunteers were recruited by the Department of Gastroenterology, Pneumology and Endocrinology and by the Department of Pediatrics at the Hospital of the Friedrich-Alexander-University, Erlangen, Germany.

Sizes and body masses of the adult models were chosen according to worldwide averages of height and body mass index (BMI) (McGee 2005). German statistics were considered for the children (Kromeyer-Hauschild *et al* 2001, McDowell *et al* 2005). Since it was essential for the volunteers to remain still in the MR scanner for several hours, children with placid dispositions were chosen. The MR scans were conducted in the presence of a radiologist. The children were accompanied by a parent and, when requested, by a pediatrician. Table 1 summarizes the main characteristics of the four models.

3.1.2. MR protocol. All volunteers were scanned on a 1.5 T Siemens Magnetom Avanto Tim (Total imaging matrix) whole body scanner at the radiological department of the Hospital of the Friedrich-Alexander-University, Erlangen, Germany. The measurement protocols for the adults and the children were developed in cooperation with Siemens Healthcare, Erlangen, Germany. To optimize the signal-to-noise ratio for all scans from head to toe, Tim Multielement Matrix coils were used for the data acquisition. The scanning sequences were chosen to meet the requirements on image contrast and resolution posed by the segmentation while minimizing the measurement time. An anticholinergic agent was administered to the adults to reduce intestinal movements during the scans. For the imaging of the blood vessels of the adults, Gadofosveset (Vasovist, Bayer Healthcare, Berlin, Germany) was used as an intravascular contrast agent. For ethical reasons, the children did not receive any kind of medication. An ECG-triggered scanning sequence was used for the heart to reduce image blurring from the heart movement. Breath-hold triggering was used for the upper torso to minimize image distortion due to the respiratory movements. The remaining blurring could easily be corrected during the segmentation.

Separate scans were necessary for the arms of the adult volunteers since they did not entirely fit into the field of view (50 cm) of the scanner. Due to the necessary repositioning

of the volunteers for the separate arm scans, changes in the shape of the soft tissues of the shoulder region occurred, and were corrected during the segmentation. All images were taken in transversal orientation. The following scanning sequences were chosen:

- head: T1 weighted MPRAGE (Magnetization Prepared Gradient Echo) $0.5 \times 0.5 \times 1.0\ \text{mm}^3$ voxel size;
- thorax (and arms of children): SPACE fast turbo spin echo 3D in $0.9 \times 0.9 \times 2.0\ \text{mm}^3$ voxel size;
- intestine (adults only): an anticholinergic agent was administered to inhibit intestinal motion;
- abdominal torso, legs and feet: SPACE, fast turbo spin echo 3D in $0.9 \times 0.9 \times 2.0\ \text{mm}^3$ voxel size;
- heart: ECG-triggered mode $0.5 \times 0.5 \times 1.5\ \text{mm}^3$ voxel size;
- left and right arms (adults): SPACE fast turbo spin echo 3D in $0.9 \times 0.9 \times 2.0\ \text{mm}^3$ voxel size.

The contrast agent used for the imaging of the arteries and veins has a relatively long latency time. After its administration, two consecutive scans of the torso were performed. The first scan was acquired during the arterial first-pass of the contrast agent, such that only the arteries appeared in the images. The second scan and all subsequent scans were obtained after the contrast agent had reached equal distribution in the vascular system (steady state). These scans yield a depiction of both the arteries and the veins. The imaging sequences were as follows:

- application of intravascular contrast agent;
- first pass angiography (arteries only): FLASH3D sequence $1.0 \times 1.5 \times 1.0\ \text{mm}^3$ voxel size;
- torso: steady-state angiography (arteries and veins) with FLASH3D-VIBE sequence $1.0 \times 1.5 \times 1.0\ \text{mm}^3$;
- left and right arms: steady-state angiography (arteries and veins), FLASH3D-VIBE sequence $1.0 \times 1.5 \times 1.0\ \text{mm}^3$.

The entire scanning time including recreative breaks for the volunteers was approximately 6 h for the adults and between 90 min and 3 h for the children depending on their body sizes.

3.1.3. Positioning and scanning of the volunteers. The position of the volunteers in the scanner corresponded to an upright standing position. The arms were parallel to the body with a gap of a few centimeters between hands and hips. Legs were straightened and did not touch. The feet were articulated at an angle of approximately 90° to the calves. Keeping gaps between arms and hips avoids hot spots in the tissue due to the RF fields of the MR scanner, which is important both for the patient safety during the scans and for the simulation of the field distribution under RF exposure. Articulating the feet permits the simulation of the models under grounded conditions.

For hearing protection, ear plugs were used instead of headphones because the force of the headphones on the head tissue would lead to significant pressure marks on the ear and the surrounding soft tissue. Nevertheless, minor marks on the skin due to the stretcher, MR receiving coils and fixation tape could not be avoided completely and were corrected during the segmentation process.

3.2. Construction of the surface mesh objects

The tissues and organs in the MR images were identified by an expert team of biologists and physicians. Manual segmentation was facilitated by the software iSEG, an in-house

development (Neufeld 2008). iSEG provides a large number of different image processing algorithms, such as Live Wire (Schenk *et al* 2000), Thresholding (Suri *et al* 2002), Region Growing (Hamerly and Elkan 2002), Fuzzy Connectedness (Udupa and Saha 2003), Interactive Watershed Transformation (Hahn and Peitgen 2003), etc. Moreover, topologically flexible interpolation is available to automatically estimate organ shapes between selected slices (based on (Raya and Udupa 1990)). Figure 1 shows the segmentation of an MR image of the head of a volunteer.

About 80 different tissues and organs were identified and segmented for each model (table 2). The segmentation was carried out organ by organ or tissue by tissue. Although the image processing software significantly facilitated the segmentation process, the correct identification of tissues required 3D visualization of the organ shape. Several iterations per organ were necessary to achieve a satisfactory result. The angiographic image sets of the vessel trees supported the segmentation of the blood vessels of the two adult models. The labor intensive development of an entire model can easily exceed six person months.

After the segmentation, the tissue boundaries were reconstructed as unstructured triangulated surfaces using the marching cubes algorithm (Lorensen and Cline 1987). These surfaces still retained the resolution of the original MR images as shown in figure 2(a). They were smoothed using the spring-model and by reducing the number of surface triangles (see, e.g., (Szczerba *et al* 2007)). These steps were carried out using the software Amira 4.0[11]. Figure 2(b) shows the final smoothed surfaces.

4. Results

4.1. The Virtual Family

Figure 3 shows the four reconstructed models of the Virtual Family. A more detailed view of the skin, the muscle tissue, the inner organs, the blood vessels and the skeleton of the six-year-old boy (Thelonious) is presented in figure 4. The reconstruction of the skull and the brain (gray and white matter) of the adult male (Duke) is shown in figure 5. For the SAR evaluation during mobile phone use according to IEEE (2005), the tissues of the pinna were segmented as separate objects. Figures 4 and 5 are representative of the level of anatomical details of all four models. Table 3 lists their organ masses in comparison with the reference models of the ICRP (2002).

Since the coordinates or the topology of the computational grid, on which, e.g., the differential equations are solved, do not necessarily coincide with the coordinates of the model, the tissue properties of the different body regions must be assigned to the respective locations of the computational grid. This process is referred to as discretizing. If the position, the orientation or the resolution of a model needs to be altered, voxel models are prone to uncertainties because thin tissue regions are prone to surface defects if the resolution of the computational mesh is in the order of magnitude of the original model. To demonstrate this effect, a prevoxeled version of the surface-based model Thelonious is generated with a voxel size of 1.5 mm $\times$ 1.5 mm $\times$ 1.5 mm. The model is sampled at the voxel centers of the computational grid. Both the prevoxeled model and the original surface-based polygon mesh model are then rediscretized at a resolution of 1.6 mm $\times$ 1.6 mm $\times$ 1.6 mm, which is slightly larger than the average skin thickness of children (Snyder *et al* 1975, Seidenari *et al* 2000). Moreover, the surface-based model is meshed using the conformal technique described in (Benkler *et al* 2008). Figure 6 shows the results of the three different discretization

[11] Visage Imaging, I. n.d. Amira—Advanced 3D Visualization and Volume Modeling. Software and user's guide available from www.amiravis.com.

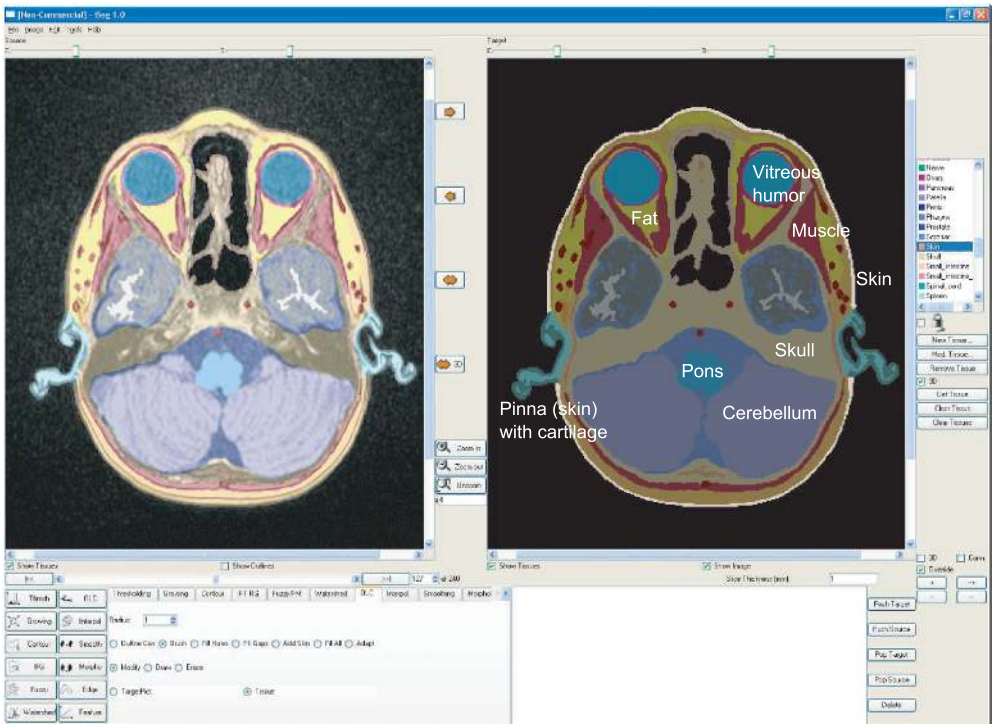

Figure 1. Segmentation of the MR images using the software iSeg.

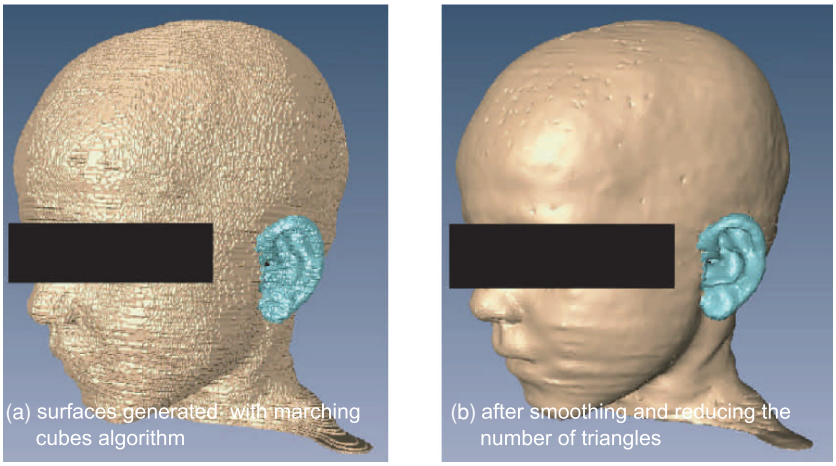

Figure 2. Reconstruction of the tissue surfaces as polygon mesh objects.

techniques. In contrast to the completely closed skin surface of the discretized polygon model, the resampled model showed significant gaps in the skin, revealing the subcutaneous tissue layers (orange). The conformal voxeling technique can render arbitrarily oriented intersections of two types of materials or tissues in the same mesh cell. This permits, for example, the smooth representation of the skin surface, and it reduces staircasing artifacts at material boundaries with high dielectric contrast.

Table 2. Segmented tissues and organs of the four models.

Tissue	Duke	Ella	Billie	Thelonious
Adrenal gland	x		x	x
Air internal	x	x	x	x
Arteries	x	x	x	x
Bladder	x	x	x	x
Blood vessel (general)	x	x	x	x
Bone	x	x	x	x
Brain (grey matter)	x	x	x	x
Brain (white matter)	x	x	x	x
Breast tissue		x		
Bronchi	x	x	x	x
Bronchi (lumen)	x	x	x	x
Cartilage	x	x	x	x
Cerebellum	x	x	x	x
Cerebrospinal fluid	x	x	x	x
Commissura anterior	x	x	x	x
Commissura posterior	x	x	x	x
Connective tissue	x	x	x	x
Cornea	x	x	x	x
Diaphragm	x	x	x	x
Epididymis	x			x
Esophagus	x	x	x	x
Esophagus (lumen)	x	x	x	x
Eye (lens)	x	x	x	x
Eye (sclera)	x	x	x	x
Eye (vitreous humor)	x	x	x	x
Fat	x	x	x	x
Gallbladder	x	x	x	x
Heart (lumen)	x	x	x	x
Heart (muscle)	x	x	x	x
Hippocampus	x	x	x	x
Hypophysis	x	x	x	x
Hypothalamus	x	x	x	x
Intervertebral disc	x	x	x	x
Kidney (cortex)	x	x	x	x
Kidney (medulla)	x	x	x	x
Large intestine	x	x	x	x
Large intestine (lumen)	x	x		
Larynx	x	x	x	x
Liver	x	x	x	x
Lung	x	x	x	x
Mandible	x	x	x	x
Marrow (red)	x	x	x	x
Medulla oblongata	x	x	x	x
Meniscus	x	x	x	x
Midbrain	x	x	x	x
Mucosa	x	x	x	x

Table 2. (Continued.)

Tissue	Duke	Ella	Billie	Thelonious
Muscle	x	x	x	x
Nerve	x	x	x	x
Ovary	n. a.	x	x	n. a.
Pancreas	x			
Patella	x	x	x	x
Penis	x	n. a.	n. a.	x
Pharynx	x	x	x	x
Pinealbody	x	x	x	x
Pinna (cartilage)	x	x	x	x
Pinna (skin)	x	x	x	x
Pons	x	x	x	x
Prostate	x	n. a.	n. a.	x
Subcutaneous adipose tissue	x	x	x	x
Skin	x	x	x	x
Skull	x	x	x	x
Small intestine	x	x	x	x
Small intestine (lumen)	x	x		
Spinal cord	x	x	x	x
Spleen	x	x	x	x
Stomach	x	x	x	x
Stomach lumen	x	x	x	x
Teeth	x	x	x	x
Tendon	x	x	x	x
Testes	x	n. a.	n. a.	x
Thalamus	x	x	x	x
Thymus	x		x	x
Thyroid gland	x	x	x	
Tongue	x	x	x	x
Trachea	x	x	x	x
Trachea (lumen)	x	x	x	x
Ureter	x	x	x	x
Uterus	n. a.	x	x	n. a.
Vagina	n. a.	x	x	n. a.
Veins	x	x	x	x
Vertebrae	x	x	x	x

The polygon mesh models are provided with a tool for arbitrary positioning and rotating with respect to the reference coordinate system. The models or parts of them can then be discretized in a rectilinear mesh at arbitrary resolution and exported in a generic voxel format (three-dimensional binary array) for use with third party simulation software. Like this, the resolution and the mesh size can be adapted to the required spatial accuracy and the available computational resources. The software and the models are provided free for research purposes[12].

[12] The order form for the models is available at http://www.itis.ethz.ch/index/index_humanmodels.html. A shipping and handling fee applies.

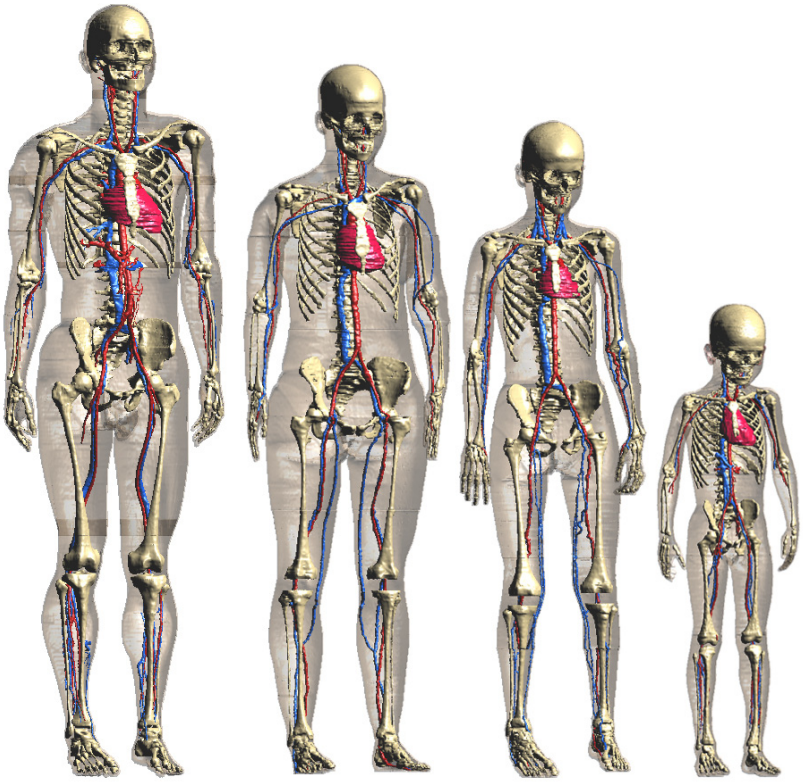

Figure 3. The Virtual Family: Duke, Ella, Billie, Thelonious (from left to right).

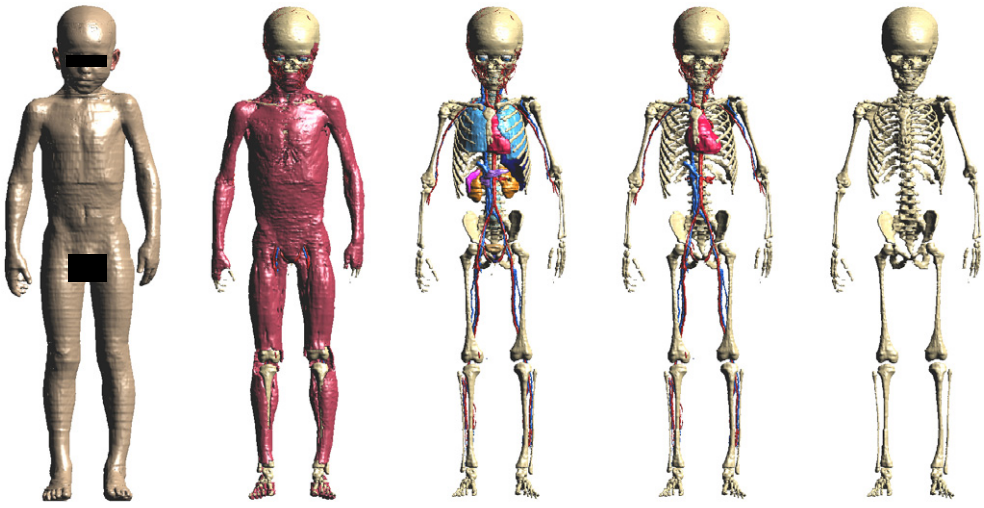

Figure 4. Thelonious: skin, muscle, inner organs, blood vessels, skeleton.

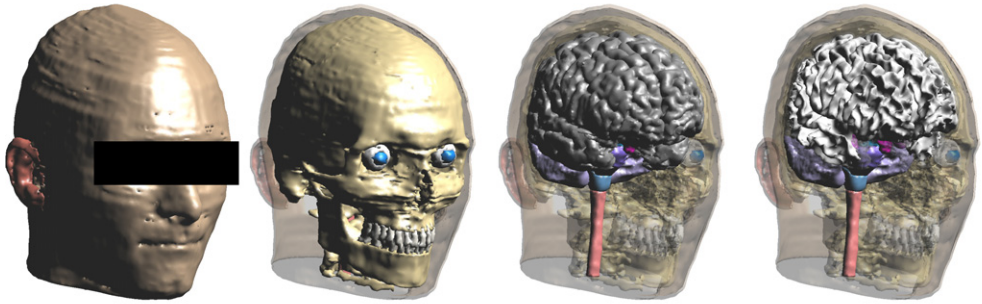

Figure 5. Duke (head only): skin, skull, brain, white matter.

Figure 6. Model Thelonious discretized at 1.6 mm voxel size: polygon mesh model voxeled (left), resampled voxel model (center), conformal voxels calculated for the polygon mesh model.

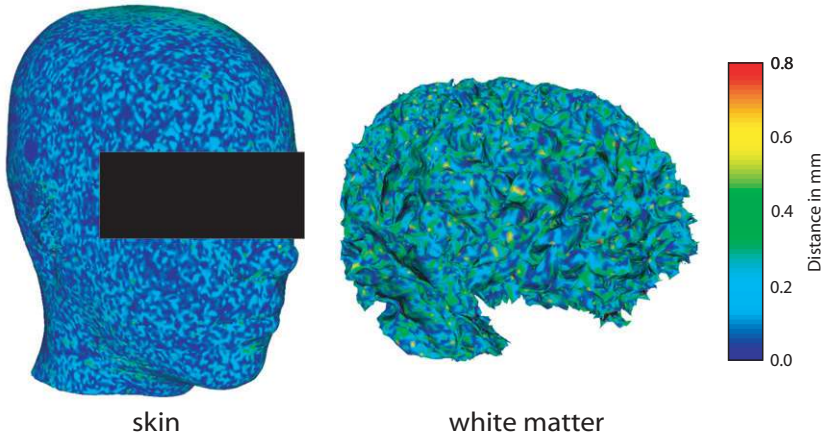

Figure 7. Two examples (skin and white matter) of the differences of the surfaces of the smoothed solids to the original segmented contours (surface normals).

Table 3. Tissue masses in g in comparison with the ICRP models (ICRP 2002).

Tissue/organ	Duke	Ella	Billie	Thelonious	ICRP Male	ICRP Female	ICRP 10 years	ICRP 5 years
Adipose tissue	11 800	14 300	5400	3600	18 200	22 500	8600	5500
Adrenals	11	–	8	3	14	13	7	5
Brain	1370	1320	1250	1310	1450	1300	1220	1180
Breast	–	490	–	–	25	500	–	–
Colon wall[a]	530	410	280	230	370	360	210	210
Eye lens	0.3	0.4	0.3	0.3	0.4	0.4	–	–
Gall bladder[b] (wall + cont.)	19	23	20	8	10 + 58	8 + 48	4.4 + 26	2.6 + 15
Heart[c]	750	790	280	260	840	620	370	220
Kidneys	360	260	170	140	310	275	180	110
Liver	1240	1100	880	570	1800	1400	830	570
Lungs[d]	3800 cm^3	2300 cm^3	1400 cm^3	900 cm^3	1200	950	500	300
Muscle	34 100	22 800	14 400	6400	29 000	17 500	1100	5600
Oesophagus (wall)	56	23	9	11	40	35	18	10
Pancreas	70	–	–	–	140	120	60	35
Red bone marrow	960	–	–	110	1170	900	630	340
Skeleton	7900	6500	5100	2500	10 500	7800	4500	2430
Skin	5500	3500	2800	1500	3300	2300	820	570
Small intestine (wall)[a]	630	270	400	60	650	600	370	220
Spleen	150	150	150	120	150	130	80	50
Testes	18	–	–	3	35	–	2	2
Teeth	31	41	32	12	50	40	30	15
Thymus	4	–	30	30	25	20	35	30
Thyroid	9	16	11	–	20	17	8	3
Uterus[a]	–	34	23	–	–	80	4	3

[a] The segmentation of the walls of the digestive tract is incomplete because of imaging limitations. This also affects the uteri of the female models (section 4.2).
[b] The wall of the gall bladder was not segmented independently from its content.
[c] Muscle and lumen.
[d] Because of the uncertainties of the density of the inflated lung tissue, the volume of the models is reported here instead of the mass. The volunteers were holding their breath during the imaging of the thorax.

4.2. Precision and limitations

In spite of the high contrast and resolution of the MR images, certain compromises during the segmentation were inevitable. Although the outlines of most of the tissues listed in table 2 could be constructed with an accuracy of 1 to 2 pixels of the original images (see section 3.1.2), the limitations of the models are as follows.

- Blood vessels with a diameter of less than 2 mm were not included.
- Nerve tissues only include the spinal cord and the optic nerve.
- In spite of the administration of the anticholinergic agent to the adult volunteers, the imaging quality of the digestive tract was not sufficient for a complete segmentation. The intestinal ducts and the lumina could not be reconstructed completely; the pancreas could only be reconstructed for the male adult model.
- The cortex of the kidneys and the walls of the stomach and the gall bladder were indistinguishable from the medulla and the lumen, respectively. They were segmented using a fixed thickness of five pixels of the MR images. The salivary glands have not been segmented separately.
- Only small fractions of the diaphragm were visible in the images. It has therefore been reconstructed with the help of anatomical atlases.
- The bone marrow of the two female models has not been segmented for the entire body. Since white and red marrow cannot be told apart in the MR images, the bone marrow has been segmented as red marrow in the male models. The periosteum has not been segmented separately for all models.
- The extrathoracic region has not been identified as a separate region.

There is good agreement between the organ masses of the ICRP reference phantoms (table 3) and the obtained models for most tissues and organs. Certain deviations can be attributed to the segmentation uncertainties—mainly of the digestive tract—as summarized above. Deviations of the masses of those tissues, which show up clearly in the MR images, are due to individual properties of the volunteers. Certain variations occur, e.g., for the spleens, the testes and the thymi of the models when compared to ICRP reference phantoms. Several studies show that they are within the statistical spread for their body weights or age groups (Markisz *et al* 1987, Schlesinger *et al* 1993, Spyropoulos *et al* 2002). During adulthood, thymic tissue is replaced by adipose tissue (Suri *et al* 1985). The segmented thymus of the Duke model corresponds to the largest contiguous section of epithelial tissue.

Additionally, the smoothing of the surfaces as discussed in section 3.2 introduces uncertainties, which are of particular relevance for thin tissue layers. The parameters of the smoothing algorithms were adjusted such that the integrity of the thin layers was retained and that complex shapes did not lose detail. This is demonstrated for a thin tissue (skin) and a complex tissue (white matter of the brain) by constructing the surface normals of each vertex of the smoothed surfaces and calculating their distances to the originally segmented outline using a highly efficient algorithm based on *kd*-trees and fast cell locators (Szczerba *et al* 2007). Figure 7 shows that the differences are generally less than 0.6 mm, which is in the order of magnitude of the resolution of the original images. As a result, introducing knowledge about the surface properties of the tissues and organs can yield a considerable improvement of the spatial resolution with respect to the resolution of the MR scans.

5. Conclusions

This paper describes the development, the accuracy and the limitations of the four anatomical whole body models (34 year old male, 26 year old female, 11 year old female, 6 year old male)

that comprise the Virtual Family. All four models and the software for their discretization (section 4.1) are freely available to the scientific community. The models are being widely applied in several studies on electromagnetic exposure, device optimization and medical applications. A few of these studies on exposure assessment (Kühn *et al* 2009), the design of hyperthermia applicators with improved performance (Christen *et al* 2008) and novel MR imaging techniques (Brunner *et al* 2009) have already been published.

Because of the large anatomical differences among individuals, the statistical relevance of computational results can only be increased by using a large number of individual models. The anatomical accuracy of the Virtual Family Models with respect to their individual features enhances the usability of the models for numerous numerical applications. The development of additional models (e.g., children of a wider age range and obese persons) and of software to articulate the limbs of the models is ongoing (Cherubini *et al* 2008). The final goal is to create a virtual population with a scope of applications ranging from fundamental research to the virtual patient and from the evaluation of the safety of physical agents to the optimization of therapeutic and diagnostic devices to improve the quality of life.

6. Disclaimer

The mention of commercial products, their sources or their use in connection with material reported herein is not to be construed as either an actual or implied endorsement of such products by the Department of Health and Human Services.

Acknowledgments

The authors acknowledge the support and expertise of Stephan Kunzelmann for the acquisition of the MR images. This work was greatly supported by Schmid & Partner Engineering AG, Switzerland, the Mobile Manufacturers Forum (MMF), Belgium and the GSM Association, Ireland.

References

Ackerman M J 1998 The visible human project *Proc. IEEE* **86** 504–11

Andreo P 1991 Monte Carlo techniques in medical radiation physics *Phys. Med. Biol.* **36** 861–920

Beard B *et al* 2006 Comparisons of computed mobile phone induced SAR in the SAM phantom to that in anatomically correct models of the human head *IEEE Trans. Electromagn. Compat.* **48** 397–407

Benkler S, Chavannes N and Kuster N 2008 Mastering conformal meshing for complex CAD-based C-FDTD simulations *IEEE Antennas Propag. Mag.* **50** 45–57

Bit-Babik G, Guy A, Chou C, Faraone A, Kanda M, Gessner A, Wang J and Fujiwara O 2005 Simulation of exposure and SAR estimation for adult and child heads exposed to radiofrequency energy from portable communication devices *Radiat. Res.* **163** 580–90

Brunner D, De Zanche N, Fröhlich J, Paska J and Pruessmann K 2009 Travelling-wave nuclear magnetic resonance *Nature* **457** 994–8

Caon M 2004 Voxel-based computational models of real human anatomy: a review *Radiat. Environ. Biophys.* **42** 229–35

Cherubini E, Chavannes N and Kuster N 2008 Realistic skeleton based deformation of high-resolution anatomical human models for electromagnetic simulations *Proc. XIX General Assembly of the Int. Union of Radio Science (URSIGA 2008) (7–16 August, Chicago, IL, USA)*

Christ A, Chavannes N, Nikoloski N, Gerber H U, Poković K and Kuster N 2005 A numerical and experimental comparison of human head phantoms for compliance testing of mobile telephone equipment *Bioelectromagnetics* **26** 125–37

Christ A, Fröhlich J and Kuster N 2002 Correction of numerical phase velocity errors in nonuniform FDTD meshes *IEICE Trans. Commun.* **E85-B** 2904–15

Christ A, Klingenböck A, Samaras T, Goiceanu C and Kuster N 2006a The dependence of electromagnetic far-field absorption on body tissue composition in the frequency range from 300 MHz to 6 GHz *IEEE Trans. Microw. Theory Tech.* **54** 2188–95

Christ A, Samaras T, Klingenböck A and Kuster N 2006b Characterization of the electromagnetic near-field absorption in layered biological tissue in the frequency range from 30 MHz to 6000 MHz *Phys. Med. Biol.* **51** 4951–66

Christen M, Schenk O and Burkhart H 2008 Alarge-scale pde constrained optimization in hyperthermia cancer treatment planning *SIAM Conf. Parallel Process. Sci. Comput.*

Dimbylow P 2002 Fine resolution calculations of SAR in the human body for frequencies up to 3 GHz *Phys. Med. Biol.* **47** 2835–46

Gabriel S, Lau R W and Gabriel C 1996 The dielectric properties of biological tissues: III. Parametric models for the dielectric spectrum of tissues *Phys. Med. Biol.* **41** 2271–93

Gandhi O, Lazzi G and Furse C 1996 Electromagnetic absorption in the human head and neck for mobile telephones at 835 and 1900 MHz *IEEE Trans. Microw. Theor. Techn.* **44** 1884–97

Hahn H and Peitgen H 2003 IWT-interactive watershed transform: a hierarchical method for efficient interactive and automated segmentation of multidimensional gray-scale images *Proc. Med. Imag.* **5032** 643–53

Hamerly G and Elkan C 2002 Alternatives to the k-means algorithm that find better clusterings *CIKM '02: Proc. 11th Int. Conf. Information and Knowledge Management (ACM, NY, USA)* pp 600–7

Hand J, Boucek J, Francis R, Jones C, Khan N, Turlach B and Green A 2008 Modelling the interaction of electromagnetic fields (10 MHz–10 GHz) with the human body: methods and applications *Phys. Med. Biol.* **53** R243–86

ICRP 2002 International Commission on Radiological Protection basic anatomical and physiological data for use in radiological protection: reference values. ICRP publication 89 *Ann. ICRP* **32** 1–277

IEC 2005 IEC 62209-1 Human Exposure to Radio Frequency Fields from Handheld and Body-Mounted Wireless Communication Devices—Human Models, Instrumentation and Procedures: Part 1. Procedure to Determine the Specific Absorption Rate (SAR) for Handheld Devices Used in Close Proximity to the Ear (Frequency Range of 300 MHz to 3 GHz) (Geneva: IEC)

IEEE 2003 IEEE 1528, Recommended Practice for Determining the Spatial-Peak Specific Absorption Rate (SAR) in the Human Body Due to Wireless Communications Devices: Measurement Techniques (Piscataway, NJ: IEEE Standards Department)

IEEE 2005 IEEE C95.1 Standard for Safety Levels with Respect to Human Exposure to Radio Frequency Electromagnetic Fields, 3 kHz to 300 GHz (Piscataway, NJ: IEEE Standards Department)

Kainz W, Christ A, Kellom T, Seidman S, Nikoloski N, Beard B and Kuster N 2005 Dosimetric comparison of the specific anthropomorphic mannequin (SAM) to 14 anatomical head models using a novel definition for the mobile phone positioning *Phys. Med. Biol.* **50** 3423–45

Kim C, Choi S, Jeong J, Lee C and Chung M 2008 HDRK-Man: a whole-body voxel model based on high-resolution color slice images of a Korean adult male cadaver *Phys. Med. Biol.* **53** 4093–106

Klemm M and Troester G 2006 EM energy absorption in the human body tissues due to UWB antennas *Prog. Electromag. Res.* **62** 261–80

Kritikos H N and Schwan H P 1976 Formation of hot spots in multilayer spheres *IEEE Trans. Biomed. Eng.* **23** 168–72

Kromeyer-Hauschild K *et al* 2001 Perzentile für den Body-Mass Index für das Kindes- und Jugendalter unter Heranziehung verschiedener deutscher Stichproben *Monatsschrift Kinderheilkunde* **149** 807–18

Kühn S, Jennings W, Christ A and Kuster N 2009 Assessment of induced radio-frequency electromagnetic fields in various anatomical human body models *Phys. Med. Biol.* **54** 875–90

Lee C, Lodwick D, Hasenauer D, Williams J, Lee C and Bolch W 2007 Hybrid computational phantoms of the male and female newborn patient: NURBS-based whole-body models *Phys. Med. Biol.* **52** 3309–33

Lorensen W E and Cline H E 1987 Marching cubes: a high resolution 3D surface construction algorithm *Proc. 14th Annual Conf. Computer Graphics and Interactive Techniques (ACM, NY, USA)* pp 163–9

Markisz J A, Treves S T and Davis R T 1987 Normal hepatic and splenic size in children: scintigraphic determination *Pediatric Radiol.* **17** 273–6

McDowell M, Fryar C, Hirsch R and Ogden C 2005 Anthropometric reference data for children and adults: US population, 1999–2002 *Adv. Data* **361** 1–5

McGee D 2005 Weight-height relationships and body mass index: some observations from the diverse populations collaboration *Am. J. Phys. Anthropol.* **128** 220–9

Neufeld E 2008 High resolution hyperthermia treatment planning *PhD Thesis* Swiss Federal Institute of Technology, Zürich (Diss. ETH No. 17947)

Neufeld E, Chavannes N, Samaras T and Kuster N 2007 Novel conformal technique to reduce staircasing artifacts at material boundaries for FDTD modeling of the bioheat equation *Phys. Med. Biol.* **52** 4371–81

Nipper J C, Williams J L and Bolch W E 2002 Creation of two tomographic voxel models of paediatric patients in the first year of life *Phys. Med. Biol.* **47** 3143–64

Patankar S V 1980 *Numerical Heat Transfer and Fluid Flow* (New York: Hemisphere)
Raya S and Udupa J 1990 Shape-based interpolation of multidimensional objects *IEEE Trans. Med. Imaging* **9** 32–42
Schenk A, Prause G and Peitgen H 2000 Efficient semiautomatic segmentation of 3D objects in medical images *Lecture Notes in Computer Science (*vol 1935*)* (Berlin: Springer) pp 186–95
Schlesinger A E, Edgar K A and Boxer L A 1993 Volume of the spleen in children as measured on CT scans: normal standards as a function of body weight *Am. J. Roentgenol.* **160** 1107–9
Schwan H P and Li K 1956 Hazards due to total body irradiation *Proc. IRE* **44** 2058–62
Segars W P, Lalush D S and Tsui B M W 1999 A realistic spline-based dynamic heart phantom *IEEE Trans. Nucl. Sci.* **46** 503–6
Segars W 2001 Development of a new dynamic NURBS-based cardiac-torso (NCAT) phantom *Doctoral Dissertation* The University of North Carolina, Chapel Hill
Segars W P, Lalush D S and Tsui B M W 2001 Modeling respiratory mechanics in the MCAT and spline-based MCAT phantoms *IEEE Trans. Nucl. Sci.* **48** 89–97
Seidenari S, Giusti G, Bertoni L and Magnoni C 2000 Thickness and echogenicity of the skin in children as assesseed by 20 MHz ultrasound *Dermatology* **201** 218–22
Shapiro A R, Lutomirski R F and Yura H T 1968 Induced fields and heating within a cranial structure irradiated by an electromagnetic plane wave *IEEE Trans. Microw. Theory Tech.* **19** 187–96
Snyder W S, Cook M J, Nasset E S, Karhausen L R, Howells G P and Tipton I H 1975 Report of the Task Group on Reference Man *ICRP Publication 23* 1st edn (New York: Elsevier)
Spyropoulos E, Borousas D, Mavrikos S, Dellis A, Bourounis M and Athanasiadis S 2002 Size of external genital organs and somatometric parameters among physically normal men younger than 40 years old *Urology* **60** 485–9
Staton R, Pazik F, Nipper J, Williams J and Bolch W 2003 A comparison of newborn stylized and tomographic models for dose assessment in paediatric radiology *Phys. Med. Biol.* **48** 805–20
Steinmann G G, Klaus B and Müller-Hermelink H K 1985 The involution of the ageing human thymic epithelium is independent of puberty: a morphometric study *Scand. J. Immunology* **22** 563–75
Suri J S, Lio K, Singh S, Laxminarayan S N, Zeng X and Reden L 2002 Shape recovery algorithms using level sets in 2D/3D medical imagery: a state-of-the-art review *IEEE Trans. Inf. Technol. Biomed.* **6** 8–28
Szczerba D, McGregor R and Szekely G 2007 High quality surface mesh generation for multi-physics bio-medical simulations *Lecture Notes in Computer Science (*vol 4487*)* (Berlin: Springer) pp 906
Udupa J K and Saha P K 2003 Fuzzy connectedness and image segmentation *Proc. IEEE* **91** 1649–69
Wiart J, Hadjem A, Gadi N, Bloch I, Wong M F, Pradier A, Lautru D, Hanna V F and Dale C 2005 Modeling of RF head exposure in children *Bioelectromagnetics* **26** (Suppl. 7) S19–30
Wiart J, Hadjem A, Wong M F and Bloch I 2008 Analysis of RF exposure in the head tissues of children and adults *Phys. Med. Biol.* **53** 3681
Xu X G, Chao T and Bozkurt A 2000 VIP-man: an image-based whole-body adult male model constructed from color photographs of the visible human project for multi-particle Monte Carlo calculations *Health Phys.* **78** 476
Xu X G and Shi C 2005 Preliminary development of a 4D anatomical model for Monte Carlo simulations *Proc. 2005 Topical Meeting. The Monte Carlo Method: Versatility Unbounded in a Dynamic Computing World (Chattanooga, TN)* (La Grange Park, IL: American Nuclear Society)
Xu X G, Taranenko V, Zhang J and Shi C 2007 A boundary-representation method for designing whole-body radiation dosimetry models: pregnant females at the ends of three gestational periods-P3, -P6 and -P9 *Phys. Med. Biol.* **52** 7023–44
Yee K S 1966 Numerical solution of initial boundary value problems involving Maxwell's equations in isotropic media *IEEE Trans. Antennas Propag.* **14** 585–9
Zaidi H and Xu X G 2007 Computational anthropomorphic models of the human anatomy: the path to realistic monte carlo modeling in radiological sciences *Annu. Rev. Biomed. Eng.* **9** 471–500
Zankl M, Fill U, Petoussi-Henss N and Regulla D 2002 Organ dose conversion coefficients for external photon irradiation of male and female voxel models *Phys. Med. Biol.* **47** 2367–85
Zankl M, Becker J, Fill U, Petoussi-Henss N and Eckermann KF 2005 GSF male and female adult voxel models representing ICRP reference man: the present status *Proc. 2005 Topical Meeting. The Monte Carlo Method: Versatility Unbounded in a Dynamic Computing World (Chattanooga, TN)* (La Grange Park, IL: American Nuclear Society)